Regulation of ATAD2B bromodomain binding activity by the histone code

Margaret Phillips[1,2], Kathleen Quinn[3], Hana Paculova[3], Cameron Montgomery[2], Faith M. Joseph[4,5], Samuel P. Boyson[2], Sunsik Chang[2], Jay C. Nix[6], Nicolas L. Young[4,5], Seth E. Frietze[3] and Karen C. Glass[1,2*]

[1]Department of Pharmacology, Larner College of Medicine, University of Vermont, Burlington, VT, 05405, USA
[2]Department of Pharmaceutical Sciences, Albany College of Pharmacy and Health Sciences, Colchester, VT, 05446, USA
[3]Department of Biomedical and Health Sciences, University of Vermont, Burlington, VT, 05405, USA
[4]Verna & Marrs McLean Department of Biochemistry & Molecular Biology, Baylor College of Medicine, Houston, TX, 77030, USA
[5]Translational Biology and Molecular Medicine Graduate Program, Baylor College of Medicine, Houston, TX, 77030, USA
[6]Molecular Biology Consortium, Advanced Light Source, Berkeley, CA, 94720, USA

* To whom correspondence should be addressed. Tel: +1(802) 656-5760; Fax: +1(802) 656-4523; Email: Karen.Glass@med.uvm.edu

ABSTRACT

The ATPase family, AAA domain containing 2B (ATAD2B) protein has a C-terminal bromodomain that functions as a 'reader' of acetylated lysine residues on histone proteins. However, the molecular mechanisms by which it recognizes chromatin with multiple post-translational modifications remain poorly understood. To gain insights into the recognition of acetylated lysines by the ATAD2B bromodomain, we investigated the recognition of combinatorial histone H4 post-translational modifications using structural and functional approaches. Using isothermal titration calorimetry, we assessed the binding affinities of the ATAD2B bromodomain with distinct histone H4 peptides harboring multiple modifications. Our results show that the ATAD2B bromodomain selectively

recognizes acetyllysine residues amongst multiple histone H4 modifications. Most of these adjacent modifications are permissive and exhibit distinctive binding affinities, however, some combinations weaken the acetyllysine interaction. Three novel protein-ligand structures reveal a unique binding mode for the ATAD2B bromodomain compared to the ATAD2 bromodomain, and highlight distinctive residues involved in the coordination of acetylated lysines in the context of adjacent post-translational modifications. To investigate the association of ATAD2B with chromatin, we performed CUT&RUN experiments in human breast cancer cells and compared the genome-wide chromatin binding sites to different regulatory histone modifications. Our results support an association of ATAD2B with endogenous acetylated histone H4. Overall, our study highlights how the interplay between various histone modifications, and combinations thereof, impact the 'reader' activity of the ATAD2B bromodomain.

INTRODUCTION

DNA is tightly packaged within the eukaryotic nucleus in the form of chromatin. The primary units of chromatin are nucleosomes, which are comprised of ~146 base pairs of DNA wrapped around an octamer of histone proteins that includes two copies of each of histone H3, H4, H2A, and H2B(1-3). Histone proteins are subject to a wide variety of post-translational modifications (PTMs) by the enzymatic addition of covalent chemical groups to their globular domain and to the amino-terminal tails that extrude from the nucleosome core particle There are many different histone PTMs, including methylation, phosphorylation, acetylation, ubiquitylation, SUMOylation, glycosylation, and ADP-ribosylation, that govern different biological processes through the regulation of chromatin structure and function (4,5). Distinctive combinations of multiple types of histone PTMs can be present simultaneously on histones, commonly referred to form a 'histone code' (6). These unique patterns of histone PTMs can serve as binding sites for a variety of effector proteins that can translate the histone code into biological readouts that include the activation and repression of the gene expression (6-8). Despite intensive research to understand the different histone 'reader' proteins that selectively recognize individual PTMs, little is known about the combinatorial recognition of different histone modifications.

Among the protein 'reader' domains known to bind to the various histone PTMs, bromodomains are acknowledged as the primary reader of acetylated lysine residues (9). Histone acetylation is recognized to regulate the relaxation of chromatin structure via repulsive electrostatic interactions between the negative charges on the acetyl group and the DNA phosphodiester backbone, permitting the accessibility of sequence-specific transcription factors to the DNA (10,11). Histone acetylation also serves as a docking site for the recruitment and assembly of protein complexes at distinct regulatory elements within the chromatin (12-14). The histone PTM ligand binding specificity of bromodomains is dictated by both the amino acid sequence surrounding the acetyllysine modification on the histone as well as the residues lining the bromodomain pocket (15). While high-resolution structures of different bromodomains in combination with acetylated histone ligands have provided critical insight into ligand recognition, the impact of combinatorial patterns of different PTMs on histone ligand selectivity remains uncharacterized.

ATAD2 and ATAD2B are two highly similar bromodomain-containing proteins that harbor conserved AAA+ ATPase domains (**A**TPases **A**ssociated with diverse cellular **A**ctivities) (16). ATAD2 and ATAD2B are paralogs and share a high degree of amino acid similarity (97% similarity in the ATPase domains and 74% in the bromodomains (17)). Their bromodomains also have similar ligand binding preferences and recognize mono- and di-acetylated lysine residues on histone H4 lysine 5 and 12 (18-21). Importantly, this H4K5acK12ac modification is often associated with newly synthesized histone H4 (22). While ATAD2 has been demonstrated to serve as a chromatin-binding protein and current research indicates it functions in the regulation of chromatin structure and transcription (19,20), the function of ATAD2B remains elusive.

In this study, we investigated the selectivity of the ATAD2B bromodomain for different H4 ligands containing multiple combinations of PTMs, including several acetylated lysines adjacent to phosphorylation or methylation marks. Using crystallographic structural analysis of the bromodomain in a complex with multiply modified histone peptides, we solved three novel high-resolution structures of the ATAD2B bromodomain in complex with histone H4 ligands, which reveal how adjacent modifications impact bromodomain recognition. To evaluate the binding of ATAD2B in the context of cellular chromatin, we performed genome-wide chromatin binding analysis of ATAD2B in human breast cancer

cells. Our results show that ATAD2B binding is strongly correlated with its preferred acetylated lysine modifications on histone H4. Altogether, these results provide new insights into the interaction of the ATAD2B bromodomain with histone H4 PTMs and highlight the potential for combinations of histone modifications to regulate bromodomain selectivity.

MATERIALS AND METHODS

Plasmid construction

The ATAD2B bromodomain-containing protein (residues 953−1085, Uniprot code: Q6PL18) was cloned into a pGEX-6P-1 plasmid containing an N-terminal GST tag and a precision protease cleavage site followed by the bromodomain sequence. GenScript performed codon optimization, gene synthesis, and subcloning into pGEX-6P-1. The plasmid was then transformed into *Escherichia coli* BL21(DE3) pLysS competent cells (Novagen) for protein expression.

Protein expression and purification

GST-ATAD2B bromodomain-containing BL21(DE3) pLysS cells were grown following our previously established protocol (21). Briefly, the transformed cells were grown at 37 °C in 2 - 4 L of Terrific broth (TB) media supplemented with ampicillin and chloramphenicol antibiotics. The cells were grown to an $O.D._{600}$~ 0.6 before induction with 0.25 mM isopropyl β-D-1-thiogalactopyranoside (IPTG), and then grown at 18°C overnight. Next, the cells were harvested at 5,000 RPM for 10 min at 4°C. The cell pellet was then suspended in 100 mL of lysis buffer (50 mM Tris−HCl pH 7.5, 500 mM NaCl, 0.05% Nonidet P-40 alternative, 1 mM dithiothreitol (DTT)) containing 0.1 mg/mL of lysozyme, and 1 tablet of protease inhibitor (Pierce protease inhibitor tablets, EDTA-free, Thermo Fisher). The cells were lysed by sonication, and cell lysate was centrifuged at 10,000 g for 30 mins. The supernatant was incubated with glutathione agarose resin (Thermo Scientific) at 4°C with gentle agitation for 1 h. The suspension was poured into 25 mL Econo-Column Chromatography Columns (Bio-Rad) and washed with ten times the resin volume of wash buffer (20 mM Tris−HCl, pH 7.5, 500 mM NaCl, 1 mM DTT). For the GST-tagged ATAD2B BRD, the protein was eluted using 50 mM reduced glutathione and

dialyzed into 20 mM sodium phosphate buffer, pH 7.0, 150 mM NaCl, and 1 mM DTT. For ITC and X-ray studies, the GST tag was cleaved off by incubating the washed beads in wash buffer supplemented with PreScission Protease (~100 μL at 76 mg/mL) (GE Healthcare) overnight at 4°C. The eluted ATAD2B bromodomain protein was concentrated to a total volume of approximately 3 mL. Protein purity and concentration were assessed as described previously (21). For western blot analysis, the cleaved GST tag was collected from the beads by eluting with 50 mM reduced glutathione and dialyzed into 20 mM sodium phosphate buffer, pH 7.0, 150 mM NaCl, and 1 mM DTT.

Histone peptide synthesis

All histone H4 N-terminal tail peptides with and without modifications were purchased from GenScript. Amino-acid sequence information of each peptide is available in **Table 1**. All peptides were synthesized with N-terminal acetylation (Nα-ac) and a free C-terminus, and were purified by HPLC to 98% purity. Mass Spectrometry was used to confirm their identity.

Isothermal titration calorimetry

For isothermal titration calorimetry (ITC), the protein was dialyzed for 48 h into 20 mM sodium phosphate buffer, pH 7.0, 150 mM NaCl, and 1 mM tris(2-carboxyethyl) phosphine (TCEP) (Thermo Scientific) and protein concentration was estimated using a NanoDrop ND-1000 spectrophotometer at A_{280} nm. The ITC experiments were carried out at 5°C using a MicroCal iTC200 or a MicroCal PEAQ-ITC instrument (Malvern Paralytical). The calorimetric titrations were performed with each histone tail ligand in the syringe (at concentrations of 2.5 mM or 5 mM) and with the ATAD2B bromodomain-containing protein in the sample cell (at concentrations ranging from 0.05 mM to 0.2 mM). The histone ligand was added to the sample cell through a series of 20 individual 2 μL injections that were spaced at time intervals of 150 s while maintaining a continuous stirring speed of 750 RPM. These were preceded by a 0.4 μL preliminary injection of the peptide ligand, which was excluded from the data integration and binding constant calculation. Control runs of histone peptide into the protein buffer were conducted under identical conditions and subtracted from the ligand into protein runs to correct for the heat

of dilution for each peptide. MicroCal PEAQ-ITC software was used for data analysis, and all data were fitted using a single set of binding sites model to calculate the stoichiometry (N) and the binding constant (K_D). All experiments in which binding occurred were performed in triplicate, while runs with no binding were performed in duplicate. To calculate the K_D, the average of the three runs was taken as the mean K_D, and the standard deviation was calculated from the mean. All values of K_D values and standard deviations for each ligand tested are reported in **Table 1**.

X-ray crystallography and structure determination

The ATAD2B bromodomain was further purified for all crystallization experiments through size exclusion chromatography using a Superdex 75 16/60 Sephacryl S-100 high-resolution gel filtration column (GE/Cytiva) on an ÄktaPrime system (GE/Cytiva). Purified ATAD2B BRD was dialyzed into 25 mM N-(2-hydroxyethyl)- piperazine-N′-ethane sulfonic acid (HEPES) buffer at pH 7.5, 150 mM NaCl, and 1 mM DTT, and then concentrated to 15 mg/mL with Amicon® Ultra (MILLIPORE) concentrators with a 3 kDa MW cut-off (3 MWCO), and the protein concentration was estimated using a UV-Vis spectrophotometer at A_{280} nm. The BRD-histone ligand complex was prepared in a 1:10 molar ratio with the bromodomain at 10 mg/mL (0.64 mM) and ligand at 6.4 mM, respectively, and stored on ice before setting up crystallization screens.

For the ATAD2B-H4K12ac (4-17) complex, sitting-drop trays were set up using the Hampton Research Index HT screen in a 96-well VDX plate (Hampton Research, Aliso Viejo, CA, USA) at 4°C. Each 2 μL drop contained 0.5 μL of the complex and 1.5 μL of the mother liquor with a 25 μL reservoir volume. Cryoprotection was achieved by dragging the crystal through LV oil added to the drop. The crystal used for the structure solution grew in 1.8 M ammonium citrate tribasic at pH 7.0 and was mounted on B1A (ALS style) reusable goniometer bases inserted with a 75 μm Dual Thickness Microloop LD built on 18 mm / SPINE length rods (pins) from MiTeGen (Ithaca, NY, USA).

For the ATAD2B-H4S1phK5ac (1-15) complex, sitting drop trays were set up using the Hampton Research Index HT screen in a 96-well VDX plate at 4°C. The 2 μL crystal drop contained 0.5 μL of the complex and 1.5 μL of the mother liquor with a 25 μL reservoir volume. The crystal was harvested using a 300 μm Dual Thickness Microloop

LD built on an 18 mm / SPINE length rod (pin) with a B1A (ALS style) reusable goniometer base from MiTeGen. The final crystal was obtained from a condition containing 0.2 M ammonium sulfate, 0.1 M BIS-TRIS (pH 5.5), 25% w/v PEG 3350, and was cryoprotected by sweeping the crystal in the loop through LV oil.

For the ATAD2B-H4S1CK5ac (1-15) complex, a sitting drop tray was set up using the Hampton Research Index HT screen, in a 96-well VDX plate at 4°C. The crystal used for structure determination grew in 0.2 M Ammonium sulfate, 0.1 M Tris pH 8.5, 25% w/v PEG 3350. Each drop was 2 μL volume made from 0.5 μL of the complex and 1.5 μL of the mother liquor with a 25 μL reservoir volume. The crystal was harvested using a 200 μm Dual Thickness Microloop LD built on an 18 mm / SPINE length rod (pin) inserted in a B1A (ALS style) reusable goniometer base from MiTeGen. An LV oil sweep was used for cryoprotection.

Data collection was carried out at the Advanced Light Source at the Lawrence Berkeley National Lab on beamline 4.2.2, which is equipped with an RDI CMOS-8M detector. The diffraction data were processed using XDS (23), and the structure was solved by a molecular replacement using PHASER (24). For all structures, the starting model was a structure of the apo ATAD2B BRD, PDB ID: 3LXJ (25). After obtaining an initial solution, several rounds of structure refinement and building were carried out with PHENIX-1.19.2 (26) and COOT 0.8.9.3. A structural model of the ATAD2B bromodomain in complex with the histone ligands was built into the composite omit map, which showed clear density for the ligand using COOT 0.8.9.3 (27), followed by iterative rounds of refinement and rebuilding in PHENIX-1.19.2 (26) and COOT 0.8.9.3. The final structures were solved at 2.0 Å resolution for ATAD2B-H4K12ac (4-17), at 1.4 Å for ATAD2B-H4S1phK5ac (1-15), and at 2.7 Å for ATAD2B-H4S1CK5ac (1-15) and were deposited into the Protein Data Bank under PDB IDs: 8EOQ, 8ESJ and 7TZQ, respectively, after validation using MolProbity (28). The hydrogen bonds and hydrophobic interactions were determined using the PLIP (29) program.

MCF7 mammalian cell culture and acid extraction of histones

MCF7 breast cancer cells were grown in in Phenol Red DMEM (Cytiva, cat. no. SH30243.FS) supplemented with a 1% Penicillin-Streptomycin cocktail and 10% heat-

inactivated FBS (Corning). Cells at 70 - 80% confluency were used for histone extraction by removing media, adding 5 mL Accutase (Innovative cell technologies), and incubating for 5 mins. The cells were collected by centrifugation at 500 g for 5 mins at 4°C, and the cell pellet was washed twice with cold PBS supplemented with 10 mM sodium butyrate. The final cell pellet was collected after centrifugation at 17,000 g for 2 mins at 4°C, was snap-frozen in liquid nitrogen and stored at -80°C.

Histones were extracted using a previously described protocol (30). Briefly, cell pellets were thawed on ice and combined with the nuclei isolation buffer (NIB) (15 mM Tris-HCl at pH 7.5, 60 mM KCl, 15 mM NaCl, 5 mM $MgCl_2$, 1 mM $CaCl_2$, 250 mM sucrose, 1 mM DTT, 0.5 mM phenylmethylsulfonyl fluoride (PMSF), 0.3% NP-40 alternative and 10 mM sodium butyrate) to a final ratio of 1:10, respectively (e.g. for every 100 μL cell pellet 1000 μL of NIB buffer was added). After gentle mixing by pipetting, the cells were placed on ice for 5 min. Nuclei were pelleted at 600 g for 5 min at 4°C. The supernatant was discarded, and the pellet was redissolved in the NIB buffer without NP-40 to a final ratio of 10:1 of buffer to pellet. The nuclei were pelleted at 600 g for 5 min at 4°C. This step was repeated three times to remove any detergents, and the final pellet was collected at max speed (15,000 to 21,000 × g) for 5 min at 4°C. Acid extraction of histones was performed by adding cold 0.2 M hydrochloric acid to the pellet with gentle mixing at a final ratio of 5:1 of acid to pellet. After incubation on ice for 5 min, the sample was centrifuged at max speed for 5 min at 4°C. The supernatant was transferred to a fresh tube and cold trichloroacetic acid (TCA) at 1 mg/mL was added to a final volume of one-quarter of the supernatant and vortexed to ensure thorough mixing. After incubation on ice for 5 min, the sample was centrifuged at max speed again for 5 min at 4°C. The supernatant was discarded, and cold, 0.1 mL acetone with 0.1% HCl was added to the precipitate. After 2 min of centrifugation at max speed, the supernatant was carefully removed by aspiration. This step was repeated using cold, pure acetone and a speed vac was used to ensure all the acetone was evaporated. The histones were redissolved in 20 mM sodium phosphate buffer, pH 7.0, 150 mM NaCl and 1 mM DTT and centrifuged at >17,000 g for 5 mins to remove any insoluble components. The supernatant was used for histone protein concentration estimation using the Bradford Assay (Bio-Rad).

LC-MS/MS

Cell pellets were collected from plates of MCF-7 cells and the histones were acid extracted after nuclei isolation as described above and previously in (30). Isolated histones were then resuspended in 85 μL 5% acetonitrile and 0.2% trifluoroacetic acid (TFA) to prepare for high-performance liquid chromatography (HPLC) separation. The histones were separated by type into families and specific variants as described previously (Holt et al., 2021). Briefly, Reverse Phase HPLC fractionation was performed with a Thermo U3000 HPLC system (Thermo Fisher Scientific, Waltham, MA) with a 150 × 2.1–mm Vydac 218TP 3-μm C18 column (HiChrom, Reading, UK, part. no. 218TP3215), using a linear gradient at a flowrate of 0.2 mL/min from 25% B to 60% B for 60 min. The composition of buffers used were A: 5% acetonitrile and 0.2% TFA; B: 95% acetonitrile and 0.188% TFA. After chromatographic separation and histone fraction collection, histone H4 was selected for further study, dried down and resuspended in additional MS buffer A (2% acetonitrile, 0.1% formic acid) for mass spectrometric analysis.

Dried H4 fractions were then diluted using the following calculation, μg H4 = (Peak area –6.0114)/31.215 to calculate the dilution to 200 ng H4/μL in MS buffer A (2% acetonitrile, 0.1% formic acid). 1 μL (200 ng) histone H4 was then loaded onto a 10 cm, 100 μm inner diameter C3 column (ZORBAX 300SB-C3 300 Å 5 μm) for online high-performance liquid chromatography (HPLC) on a Thermo U3000 RSLC nano Pro-flow system. A 70-minute linear gradient using buffer A: 2% acetonitrile, 0.1% formic acid, and B: 98% acetonitrile and 0.1% formic acid was used, and the samples were maintained at a temperature of 4°C. The column eluant was introduced into a Thermo Scientific Orbitrap Fusion Lumos by nanoelectrospray ionization. A static spray voltage of 1800 V and an ion transfer tube temperature of 320°C were set for the source. The MS1 experiment used a 60 k resolution setting in positive mode. An AGC target of 5.0e5 with 200 ms maximum injection time, three micro scans, and a scan range of 700-1400 m/z were used. A targeted charge state of +15 was selected for histone H4. An intensity threshold of 1e5 was set for the selection of ions for fragmentation. The target precursor selected for MS2 fragmentation included all major H4 peaks and chose the top 20 most abundant m/z. ETD fragmentation at a 14 ms reaction time, 5.0e5 reagent target with 200 ms injection time

was used. MS2 acquisition was performed using the orbitrap with the 60 k resolution setting, an AGC target of 5.0e5, a max injection time of 200 ms, a 'normal' scan range, and three micro scans.

H4 proteoform quantitation

Identification of H4 at the desired charge state of +15 was observed in mass spectra. Raw files were converted to mzXML. Data processing was performed by a custom analysis suite as previously described (30,31).

Histone Pull-down assay

20 μM of the GST-tagged ATAD2B bromodomain in 20 mM sodium phosphate buffer, pH 7.0, 150 mM NaCl, and 1 mM DTT was incubated with 50 μg of histones extracted from the above step with gentle shaking for 1 hour at 4°C. To rule out non-specific interactions with the GST tag, a GST control was set up with 50 μg of extracted histones incubated with 20 μM of GST alone for 1 hour at 4°C with gentle shaking.

To isolate the ATAD2B bound histones 50 μL of Pierce glutathione agarose (Thermo Scientific) was pre-equilibrated in the same buffer as the protein and incubated with the GST-ATAD2B and histone complex for 1 hour at 4°C with gentle shaking. Samples were spun down at 500 g for 2 mins and the supernatant was discarded. The beads were washed thrice with 500 μL of wash buffer (20 mM sodium phosphate buffer, pH 7.0, 150 mM $NaCl_2$, 1 mM DTT, and 1.0% NP-40 alternative) each time with gentle mixing and spun down at 500 g for 2 mins to remove the wash supernatant. Finally, 50 μL of 2X Laemmle sample buffer (supplemented with 2-Mercaptoethanol, Bio-Rad) was added to the beads and boiled for 5 mins at 95°C. The beads were spun down at >17,000 g for 5 mins, and the supernatant was loaded onto a 4-15% precast SDS-PAGE gel (Mini-PROTEAN, Bio-Rad) and run at 100 V for 1.5 h. The gel was then transferred to a 0.45 mM PVDF membrane (Thermo Scientific) at 100 V for 1 h at 4°C. The membrane was first rinsed in TBST buffer (50 mM Tris pH 7.4, 150 mM NaCl, and 0.1% Tween-20) and then blocked with 5% BSA (bovine serum albumin, Thermo Scientific) shaking at 4°C for 1 h. The membrane was rinsed three times (5 mins each) with TBST buffer. Immunoblotting was performed using the following antibodies: anti-GST (ABclonal, Cat.

No. AE006), anti-H4K5ac (EpiCypher, Cat. No. 13-0051), and anti-H4K12ac (EpiCypher, Cat. No. 13-0037). Antibody incubations were carried out for 16 h overnight at 4°C with gentle rocking. The membranes were then rinsed three times (10 mins each) with TBST buffer before incubation with HRP-conjugated secondary antibody (ECL Anti-Rabbit IgG, Cytiva) in 2.5% BSA for 1 hour at 4°C. After rinsing the membrane three times (5 mins each) with TBST buffer, chemiluminescence was used for protein visualization using the SuperSignal West Pico PLUS substrate (Thermo Scientific) following the manufactures protocol.

CUT&RUN

CUT&RUN experiments were performed in the MCF7 cell line, using specific antibodies for the following proteins: ATAD2B (Invitrogen, Catalog # PA5-83233, Lot:), histone H4K5ac (Invitrogen, Ref # MA-32009; Lot:), histone H4K8ac (Epicypher Ab - Ref. 13-0036; Lot:), and histone H4K12ac (EpiCypher, SKU:13-0037, Lot:). Biological replicates were generated for ATAD2B. Cells were harvested at ~70-80% confluency, and the samples were prepared following the EpiCypher CUTANA ChIP/CUT&RUN Kit protocol (Epicypher, SKU: 14-1048) with minor adjustments, including adding 5 mM sodium butyrate and 1uM trichostatin-A to the wash and antibody buffers. An IgG antibody served as a negative control to evaluate non-specific background signal from chromatin captured during immunoprecipitation, and an *E. Coli* spike-in control was added for normalizing enrichment during analysis. CUT&RUN libraries were prepared according to the NEBNext Ultra II DNA Library Kit for Illumina, and each sample was uniquely barcoded with the NEBNext Multiplex Oligos for Illumina. Minor adjustments in library preparation included changes in PCR cycling parameters and library clean-up as described in the EpiCypher protocol. Libraries were pooled and sequenced using 75 base pair paired-end reads on the NextSeq 500 High Output platform obtaining a sequencing depth of at least 10 million reads per sample. CUT&RUN data analysis was performed using the CUT&RUNTools pipeline (32), including Bowtie2 to map reads to the human reference genome (hg38) and MACS2 for calling peaks (33,34). The Seqsetvis and ssvQC packages were used to evaluate replicate concordance, quality control, and visualization (35). ATAD2B correlation analysis with histone PTMs was performed using the diffbind R package (36)

with the top 20% of peaks for all datasets. ChIP-seq datasets were downloaded from the ENCODE portal (https://www.encodeproject.org/) (37,38) accessions: ENCFF714DEQ, ENCFF378IVZ, ENCFF959VSM, ENCFF348DEB, ENCFF660MSN, ENCFF991HJA, ENCFF188VRU, ENCFF268RXB, ENCFF518MOR, ENCFF595UXF, ENCFF538BHD, ENCFF340KSH, ENCFF739SBL). The H4K5ac, H4K8ac, and H4K12ac were generated by CUT&RUN analysis as described above.

RESULTS

Combinatorial histone PTMs influence ligand recognition by the ATAD2B bromodomain

Our prior studies compared the histone modifications recognized by the ATAD2 and ATAD2B bromodomains using an unbiased histone PTM ligand binding screen containing 288 distinctive peptides with both single and combinatorial histone modifications (21). We found that the ATAD2B bromodomain could bind to acetylated lysine modifications within the context of other marks, including methylation and phosphorylation at sites adjacent to an acetylated lysine residue (21). We hypothesized that while the bromodomain only recognizes acetylation marks, neighboring PTMs (of varying shape, size, and charge) would influence the interaction with the acetyllysine group. Thus, we first performed quantitative histone peptide binding analysis by ITC to study the mechanisms underlying histone PTM recognition. The histone peptides used in the experiments were selected from the top histone H4 ligands (21) and have uniform amino-acid sequence lengths to allow for a direct comparison (**Table 1**, **Supp. Fig. S1**). As expected, the ATAD2B bromodomain preferentially bound histone H4K12ac (K_D = 22.84 ± 2.07 μM), and no binding was observed for H4K8ac, H4K16ac, and H4K20ac peptides. Among the di-acetylated histone peptides tested, H4K5acK12ac exhibited the highest affinity (K_D = 25.91 ± 3.96 μM), which is similar to its affinity with mono-acetylated H4K12ac. The tri-acetylated H4K5acK12acK16ac peptide bound with an affinity of K_D= 34.06 ± 6.31 μM. It is interesting to note that acetylation at K8 was less tolerated in the presence of K5 acetylation and resulted in weaker binding affinities of the H4K5acK8acK12ac (K_D= 78.30 ± 2.92 μM) and the H4K5acK8acK12acK16ac peptides (K_D = 62.77 ± 10.93 μM) compared to H4K5acK12ac and H4K5acK12acK16ac, respectively (**Table 1**).

The influence of neighboring modifications on acetyllysine recognition was most prominent when a negatively charged phosphoryl group at the N-terminus was present (H4S1phK5ac). Compared to H4K5ac with a K_D of 5.2 ± 1.0 μM (21), the binding affinity for the ATAD2B BRD with the H4S1phK5ac peptide was significantly decreased (K_D = 84.21 ± 13.12 μM). Interestingly, the presence of a hydrophobic methyl group at K8 was better tolerated than acetylation at K8, as methylated ligands exhibited an increased binding affinity with the ATAD2B BRD (compare H4K5acK8me1K12ac (K_D = 48.233 ± 2.44 μM) and H4K5acK8me1K12acK16ac (K_D = 47.93 ± 1.44 μM) with H4K5acK8acK12ac (K_D = 78.30 ± 2.92 μM) and H4K5acK8acK12acK16ac (K_D = 62.77 ± 10.93 μM). The presence of bulky di-methyl groups at R3 in H4R3me2K5ac (residues 1-24) was also permissive and did not alter the binding affinity of the ATAD2B BRD considerably (compare K_D= 55.50 ± 11.20 μM with the mono-acetylated H4K5ac K_D= 50.52 ± 4.39 μM).

Histones post-translational modifications are dynamic, and are often found in different abundances on both the N- and C-terminal regions of the histone proteins (6,39-43). The modified histone ligands in the dCypher screen were designed and synthesized to cover known post-translational modifications on the canonical and variant histones in a combinatorial manner. However, it does not necessarily represent the physiologically relevant combinations of modifications on individual histone molecules (also known as histone proteoforms) that are biologically available within the cell. To assess this, we used a top-down proteomic approach, which omits protein digestion, to identify and quantify the abundance of intact histone H4 proteoforms in MCF7 human breast cancer cells (**Table 1**, right column). These proteoform profiles confirm that mono-, di-, tri- and tetra-acetylated histone H4 are biologically relevant ligands, and that phosphorylation and methylation marks surrounding the acetylated lysine modifications are also available within these cells. Thus, the combination(s) of physiologically relevant combinations of histone PTMs likely influence the histone recognition activity of the ATAD2B bromodomain.

Molecular mechanisms of acetyllysine recognition by the ATAD2B bromodomain

While recognition of mono-acetylated histone H4 by the ATAD2 bromodomain is established (20,44), there is little information on how its ATAD2B paralog coordinates acetyllysine modifications. Thus, to elucidate the mechanisms involved in acetyllysine recognition, we co-crystallized the ATAD2B BRD with the mono-acetylated H4K12ac (residues 4-17) histone ligand. The X-ray crystal structure of this complex was solved at a resolution of 2.0 Å by molecular replacement using the apo ATAD2B-BRD crystal structure (PDB ID: 3LXJ) (**Figure 1A, Supp. Table S1**). As illustrated in the $2F_o–F_c$ composite omit map, good ligand density was observed for residues Gly 6 to Arg 17 of the histone H4 peptide within the canonical bromodomain pocket (**Figure 1B**). Multiple hydrogen bonds and hydrophobic interactions contribute to histone ligand coordination (**Figure 1C**).

As observed in **Figure 1C**, our structure reveals a canonical binding mode for the acetyllysine group defined by a hydrogen bond between the carbonyl of the acetyllysine moiety and the conserved N1038, as well as a water-mediated hydrogen bond to residue Y995 of the ATAD2B BRD. Our structure also reveals a distinct binding interactions in the ATAD2B BRD characterized by multiple hydrogen bonds formed between the histone backbone residues and the BRD ZA/BC loop residues. These include hydrogen bonds between Gly 7 and Gly 8 with the L1035 and E1036 residues, respectively, and Gly 9 and Gly 11 of the histone backbone with the Y1037 residue in the BRD pocket. Additional hydrogen bonds between Leu 10 and Arg 17 of the histone ligand to residues D994 and S993, further contribute to the histone peptide read-out. Additional specificity for the histone ligand is achieved through hydrophobic interactions between the aliphatic acetyllysine side chain and the hydrophobic ‘gatekeeper’ residue I1048, the ‘NIF’ shelf residues I982 and F983, and the ‘ZA loop’ residues V992 and V987 in the ATAD2B BRD. Overall, our crystal structure illustrates that the ATATD2B BRD adopts the canonical binding pocket for the acetylated lysine modification recognition and highlights a diverse network of polar and non-polar interactions that coordinate the recognition and selection of the H4K12ac mark.

Molecular mechanisms contributing to altered ATAD2B BRD binding affinity by adjacent histone modifications

Based on the H4K12ac structure, where several polar contacts between the histone residues surrounding the acetyllysine mark interact with BRD residues, we hypothesized that PTMs neighboring the acetyllysine mark would also influence the BRD histone peptide binding activity. We co-crystallized the ATAD2B-BRD with a histone H4 ligand (residues 1-15) containing adjacent phosphorylation and acetylation modifications (H4S1phK5ac) and solved the crystal structure at a resolution of 1.4 Å (**Figure 2A**, **Supp. Table S2**). Electron density for histone residues 1-6 was observed within the ATAD2B BRD binding pocket (**Figure 2B**). Similar to H4K12ac, coordination of the K5 acetyllysine occurs via hydrogen bonds and hydrophobic contacts to the BRD through conserved residues N1038, Y995, and the hydrophobic residues of the ZA and BC loop region, respectively. Y1037 of the BRD forms hydrogen bonds with Gly 2 and Gly 4 in the histone ligand. Notably, fewer hydrogen bond and hydrophobic interactions were observed with coordination of the H4S1phK5ac ligand than with the H4K12ac ligand, which is likely reflective of the lower binding affinity for the H4S1phK5ac ligand. Furthermore, the bulky phosphate group pushes the histone ligand backbone residues away from the BC loop. Overall, our structure of the ATAD2B BRD in complex with the histone H4S1phK5ac ligand highlights that although the coordination of the acetyllysine modifications at H4K5ac and H4K12 are conserved, the phosphorylation of Ser 1 likely introduces steric clashes that reduce the number of protein-ligand contacts, resulting in a weaker overall binding affinity.

Histone H4 mutations demonstrate altered ATAD2B bromodomain recognition

Our crystal structures of ATAD2B in complex with the H4K12ac and H4S1phK5ac ligands outline the importance of specific contacts to the histone tail backbone residues in coordinating the acetylated histone ligands. Thus, we also examined whether mutations in histone H4 residues adjacent to acetylated lysine modification could impact bromodomain binding activity. A recent study identified ‘oncohistone’ mutations in histone genes associated with cancer (45). Several oncohistone mutations occur at or adjacent to sites of known PTMs (45,46), and we selected the top four N-terminal mutations that

are close to histone H4K5 and assessed their impact on ATAD2B bromodomain binding (**Table 2, Supp. Figure S3**). Mutation of Ser 1 or Arg 3 to Cys decreased the binding affinity for the K5ac mark compared to the wild-type H4K5ac (**Table 2**) (21). Furthermore, mutation of Gly 4 to either Asp or Ser completely abolished the recognition of the K5ac group by the BRD (**Table 2**). The X-ray crystal structure of the ATAD2B bromodomain in complex with H4S1CK5ac was solved at a resolution of 2.79 Å (PDB ID: 7TZQ, **Figure 3A, Supp. Table S3**). As illustrated by the $2F_o–F_c$ composite omit map, ligand density was observed for the first seven residues of the histone peptide inside the ATAD2B BRD binding pocket (**Figure 3B**). As expected, coordination of the acetyllysine group in the ATAD2B BRD binding pocket was well conserved except for a missing water-mediated hydrogen bond between the ATAD2B BRD residue Y995 and the acetyllysine group of the H3S1CK5ac ligand (**Figure 3C**). This structure illustrates that although the K5ac coordination in the binding pocket is similar what we observed in the S1phK5ac and H4K12ac structures, the oncomutation H4S1CK5ac results in reduced interactions with the N-terminus of histone H4. Thus, our structural data, taken in conjunction with our ITC binding data, demonstrate that mutations within the histone H4 backbone decrease the affinity of the ATAD2 BRD with acetylated histone H4 ligands.

Genome-wide ATAD2B chromatin binding correlates with acetylated histone H4 modifications

To further explore the mechanisms underlying histone PTM recognition by ATAD2B, we tested whether ATAD2B could bind natively acetylated histone proteins extracted from MCF7 breast cancer cells. We expressed and purified the ATAD2B BRD as a GST-fusion protein and incubated it with histones isolated from the MCF7 cells. Acetylated histones with H4K5ac and H4K12ac modifications were pulled down by the ATAD2B bromodomain (**Figure 4A**). To investigate the association of ATAD2B with chromatin in cells, we determined the genome-wide binding sites of ATAD2B in the human breast cancer MCF7 cell line using CUT&RUN analysis. Two independent replicates identified a high degree of overlap between ATAD2B replicate datasets, demonstrating a consensus dataset of over 36,000 shared peaks (**Figure 4B** and **Supp. Figure S2**). A comparison of the ATAD2B peaks with different regulatory histone PTMs from MCF7 cells demonstrated

that the top 20% of ATAD2B peaks were correlated with the histone H4 acetyllysine modifications (H4K5ac, H4K8ac, and H4K12ac), more than any other regulatory PTM modifications in MCF7 cells (**Figure 4C**). To further examine the enrichment patterns of these H4Kac PTMs, we compared the enrichment signal of these modifications at the consensus ATAD2B binding sites (**Figure 4D**). ATAD2B showed broad enrichment patterns for several genes, including *MYC*, *E2F1*, and *BRCA1,* with similar signal enrichment patterns for ATAD2B and the H4K5ac, H4K8ac, and H4K12ac (**Figure 4E**). These results indicate that ATAD2B binds to chromatin and shares genomic enrichment patterns with multiple histone H4 PTMs known to be recognized by the ATAD2B bromodomain.

DISCUSSION

Understanding the mechanisms by which different bromodomains recognize distinctive patterns of histone modifications is essential for our understanding of their function as putative chromatin regulators. ATAD2 and its closely related paralogue ATAD2B, belong to sub-family IV of the human bromodomains (16). The bromodomains of these related proteins share a high degree of structural similarity and exhibit comparable ligand preferences for histone H4 acetylation modifications *in vitro* (20,21,42,43). Our prior study utilized a screen for different histone PTMs on histone peptides and found that both ATAD2 and ATAD2B bromodomains exhibit a preference for di-acetylated H4K5acK12ac. However, the ATAD2B bromodomain was more promiscuous, and could bind to a higher number of ligands containing distinctive arrangements of PTMs on the histone peptides including adjacent acetylation and methylation modifications (21). This suggests that structural differences between the ATAD2 and ATAD2B bromodomains contribute to distinctive histone-binding properties. These unique properties may provide insight into their unique cellular functions and will allow the development of specific agents that specifically target either protein by blocking the bromodomain acetyllysine binding activity.

ATAD2 has been widely studied in the context of cancer and is thought to be involved in chromatin remodeling activities associated with transcription, DNA damage repair, and cell cycle progression (19,20,47,48). However, the precise role for histone ligand

recognition by the ATAD2 bromodomain in these various processes remains largely uncharacterized. A recent study by Lazarchuk et al. showed that ATAD2 may play a role in DNA replication during S phase of the cell cycle by protecting newly synthesized histones containing H4K5acK12ac modifications from histone deacetylases HDAC1 and HDAC2 until they are incorporated into chromatin (49). Yet, the cellular function of ATAD2B remains uncharacterized. Understanding the similarities and differences between the ATAD2 and ATAD2B bromodomain-histone PTM interactions may shed light on the unique functions of the ATAD2B protein.

Here, we directly measured the binding affinities of the ATAD2B bromodomain to histone H4 peptide ligands containing different PTMs. Our results from ITC analysis demonstrated that the mono-acetylated H4K12ac and di-acetylated H4K5acK12ac are the preferred ligands of the ATAD2B bromodomain, exhibiting the highest affinities compared to other mono-, di-, tri-, and tetra-acetylated histone H4 PTMs (**Table 1**). Thus, the H4K12ac modification likely drives the ATAD2B bromodomain interaction with acetylated histones. The di-acetylated H4K5acK12ac modification has been identified as an abundant proteoform in acute myeloid leukemia cells (50). Moreover, this di-acetylated mark is highly enriched in newly synthesized histones found in the nascent chromatin (22,51). Interestingly, both ATAD2 and ATAD2B were found to be localized newly synthesized chromatin (52). Thus, our ITC data demonstrating a strong affinity for the histone H4K5acK12ac ligand by the ATAD2B bromodomain also supports a role for ATAD2B in the regulation of nascent chromatin via interaction with di-acetylated H4 histones.

Within the chromatin, histones often contain multiple PTMs in various combinations (53-57). Our ITC data demonstrates how multiple PTMs on the histone H4 tail modulates the ATAD2B BRD binding activity. Among the di-, tri-, and tetra-acetylated histone H4 peptides tested, acetylation at K8 had a negative effect on the histone tail recognition (**Table 1**). However, methylation at K8 was well tolerated (**Table 1**). Moreover, analysis of the ITC data show that individual PTMs adjacent to the preferred H4K5/K12 acetylation sites impact ligand recognition by the ATAD2B bromodomain. Namely, adjacent acetylation and methylation modifications are permissive in the context of ATAD2B bromodomain binding activity, whereas phosphorylation adjacent to the acetyllysine

moiety negatively impacted acetylation coordination (**Figure 5**). Structural analysis indicates that phosphorylation on Ser 1 impedes H4K5ac recognition by blocking close interactions with the N-terminal tail of Histone H4 via steric hindrance. Interestingly, histone H4 phosphorylation at Ser 1 (H4S1ph) is also associated with newly synthesized histones (58), and it is most abundant during the mitotic and S phases of the cell cycle (59). Phosphorylation of S1 on histone H4 is also induced following DNA damage and is possibly associated with DNA double-strand break repair (60). This is reminiscent of a previous study reporting inhibition of H3K9me3 recognition by the heterochromatin protein 1 (HP-1) in the presence of S10ph (61), and these studies highlight how ATAD2B activity may be modulated in the cell (**Figure 5**).

To compare the ATAD2 and ATAD2B bromodomain binding mechanisms, residue-specific information provided by our high-resolution crystal structure of the ATAD2B BRD in complex with the histone H4S1phK5ac ligand show that the K5ac insertion in ATAD2B BRD is similar to K5ac coordination by the ATAD2 BRD (PDB ID: 4QUU, 4TT2) (20,62). However, some key differences were observed between the two bromodomain structures (PDBIDs: 8ESJ and 4QUU). Notably, the orientation of the H4K5ac peptide in the ATAD2 4QUU structure is such that the N-terminal R3 residue of the histone ligand is positioned close to D1066 of the ATAD2 BRD, resulting in a hydrogen bond (20). D1066 is on the BC loop, and the hydrogen bond pulls the loop into closer contact with the histone ligand. In our ATAD2B BRD structure (**Figure 2**), the histone ligand orientation places the N-terminus residue, S1ph, away from the corresponding D1040 residue in ATAD2B, which instead forms a hydrogen bond with E1036 of the ATAD2B BRD. This leaves the BC loop in our ATAD2B BRD structure more flexible.

Furthermore, the histone H4R3 residue in the ATAD2 BRD structure (PDB ID: 4QUU) forms two water-mediated hydrogen bonds with E1062, whereas in our ATAD2B BRD structure bound to H4K5ac R3 has a flipped side-chain orientation that is closer to the ZA loop residues S993 and D994, resulting in new hydrogen bond contacts. In contrast, no hydrogen bond interactions are observed between the ZA loop residues and the H4K5ac ligand in the ATAD2 BRD structure (PDBID: 4QUU). These differences in coordination of the K5ac moiety could help explain the effects of adjacent PTMs on acetyllysine recognition by the ATAD2B BRD.

Structural analysis of the ATAD2B BRD in complex with the histone H4K12ac ligand (**Figure 1**) confirms that coordination of the acetyllysine moiety is consistent between the ATAD2 and ATAD2B BRDs (20). However, there are notable differences in interactions with the histone ligand backbone residues between the ATAD2 and ATAD2B bromodomains. In the crystal structure of the ATAD2 BRD bound to H4K12ac (PDB ID 4QUT), the histone ligand was coordinated mainly through water-mediated interactions between the protein and the histone peptide backbone except for histone residue G9, which forms hydrogen bonds with D1066 and D1071 of the ATAD2 BRD (20). In our ATAD2B BRD H4K12ac structure, an intricate network of specific contacts is observed through eight direct hydrogen bonds between the BRD residues and the histone ligand backbone (**Figure 1C**). These distinctive differences in coordination of H4K12ac by the ATAD2 and ATAD2B BRDs is indicative of unique binding modes between the two bromodomains, which is also reflected in significant differences in their binding affinity for the same PTM histone ligand.

Oncohistones have been described in various tumors where histone genes harbor mutations in regions encoding both the tail and core residues (45,46). Within histone H4, the most frequently observed mutations occur at the N-terminal tail. ATAD2B bromodomain binding analysis demonstrates that the most frequent somatic mutation, H4R3C has a negative effect on the recognition of the adjacent K5ac modification. Based on the ATAD2B BRD-H4S1phK5ac and ATAD2B BRD-H4S1CK5ac structures, the reduced binding affinity for the H4R3CK5ac ligand likely results from the loss of the positively charged R3, which no longer supports hydrogen bond formation between ZA loop residues in the BRD binding pocket and this histone H4 tail residue. Although there is a slight decrease in binding affinity, a conservative mutation of H4S1 to Cys in the H4S1CK5ac ligand does not significantly alter the coordination of H4K5ac within the ATAD2B BRD binding pocket.

We also found that the ATAD2B bromodomain can pull down endogenous histones with the H4K12ac modification (**Figure 4A**), which supports a cellular role for ATAD2B in histone H4 binding. Hyperacetylation of the histone H4 N-terminal tail has been associated with chromatin decompaction and transcriptional activation (63-66). To investigate the chromatin binding patterns of ATAD2B with various histone modifications,

we identified the genome-wide binding sites of ATAD2B in MCF7 cells, and compared the corresponding enrichment patterns to data generated by the ENCODE project (37,38). ATAD2B exhibits a genomic localization pattern that correlates with histone H4 acetylation post-translational modifications and is enriched at sites of H4K5ac, K8ac, and K12ac. Together, these data suggest the role for H4 acetyllysine PTMs in recruiting the ATAD2B protein to the chromatin to carry out its biological functions.

The interplay between diverse histone PTMs forms the 'histone code,' which drives the recruitment of reader proteins to the chromatin, and ultimately dictates specific cellular outcomes. Our current study highlights the importance of studying crosstalk between various histone post-translational modifications to understand how they modulate bromodomain binding activity. Adjacent histone PTMs can either promote or inhibit the affinity of the bromodomain module with the chromatin, which, in turn, regulates essential cellular processes such as gene transcription. Future investigations focused on revealing how individual and combinatorial histone modifications direct the localization of ATAD2B to specific regulatory sites along the genome are needed in order to understand how complex epigenetic signals created by the 'histone code' drives gene regulation in specific biological contexts. Furthermore, understanding the molecular mechanisms underlying these interactions will provide new insights for the development of therapeutic interventions to treat disease, particularly cancer. Our results on the ligand binding activity of the ATAD2B bromodomain are important for understanding the function of the ATAD2B protein in normal biological and cellular processes.

Author Contributions: Conceptualization, M.P., S.F, and K.C.G; investigation and validation, M.P., K.Q., C.M., F.J., S.B., S.C., J.N., N.L.Y., S.F., and K.C.G.; writing, M.P., reviewing, and editing M.P., K.Q., F.J., N.L.Y., S.F., and K.C.G.; supervision, S.F., N.L.Y., and K.C.G.; funding acquisition, K.C.G., and S.F. All authors have read and agreed to the final version of the manuscript.

DATA AVAILABILITY

The atomic coordinates and structure factors for the ATAD2B BRD in complex with histone H4K12ac (4-17), H4S1phK5ac (1-15), and H4S1CK5ac (1-15) have been

deposited in PDB and will be made available upon publication. The CUT&RUN data will also be made available through the NCBI GEO database upon publication.

ACCESSION NUMBERS

The atomic coordinates and structure factors for the ATAD2B BRD in complex with histone H4K12ac (4-17), H4S1phK5ac (1-15), and H4S1CK5ac (1-15) have been deposited with the Protein Data Bank under the accession numbers – 8EOQ, 8ESJ, and 7TZQ respectively.

ACKNOWLEDGMENTS

We want to thank Dr. Zhao Lai at the Genome Sequencing Facility at Greehey Children's Cancer Research Institute at UT Health San Antonio for DNA sequencing.

FUNDING

Research reported in this study was supported by the National Institute of General Medical Sciences and the National Cancer Institute of the National Institutes of Health under award numbers (R15GM104865 to KCG) and (R01GM129338, P01CA240685 to KCG and SEF). This work was also supported by National Institutes of Health grants to NLY (R01GM139295, P01AG066606, and R01CA193235). The content is solely the responsibility of the authors and does not necessarily represent the official views of the National Institutes of Health. This study used the Advanced Light Source in Berkley, CA, and the National Magnetic Resonance Facility at Madison (NMRFAM). Beamline 4.2.2 of the Advanced Light Source, a DOE Office of Science User Facility under Contract No. DE-AC02-05CH11231 is partly supported by the ALS-ENABLE program funded by the National Institutes of Health, National Institute of General Medical Sciences grant number (P30GM124169). Automated DNA sequencing was performed in the Vermont Integrative Genomics Resource DNA Facility and was supported by the University of Vermont Cancer Center, the Lake Champlain Cancer Research Organization, and the UVM Larner College of Medicine. This research was supported by an ACPHS summer research award to SC and by the UVM Larner College of Medicine.

CONFLICTS OF INTEREST

The authors declare no conflict of interest with the content of this article.

TABLES

Table 1: **ATAD2B BRD ligand binding affinities and cellular abundance of histone H4 PTMs.** The dissociation constants for the ATAD2B BRD interaction with multiple modifications on histone H4 peptides were determined by ITC. The identity and abundance of specific PTMs in MCF7 cells were carried out by mass spectrometry. All histone H4 peptides carry an N-terminal acetylation group (Nα-ac).

Peptides used for ITC	Dissociation Constant (μM)	N	% Abundance
H4 unmodified (residues 1-24)	No Binding	NA	53.17 ± 0.75
H4K5ac (1-24)	50.52 ± 4.39	1.00	3.62 ± 1.62
H4K8ac (1-24)	No binding	NA	6.69 ± 0.29
H4K12ac (1-24)	22.84 ± 2.07	1.00	8.52 ± 1.63
H4K16ac (1-24)	No binding	NA	9.77 ± 0.48
H4K20ac (1-24)	No binding	NA	*
H4K5acK8ac (1-24)	94.57 ± 17.16	1.00	2.25 ± 1.11
H4K5acK12ac (1-24)	25.91 ± 3.96	1.03	7.92 ± 0.23
H4K8acK12ac (1-24)	30.90 ± 1.55	1.00	11.95 ± 1.64
H4K12acK16ac (1-24)	35.56 ± 3.57	1.00	29.83 ± 7.03
H4K12acK20ac (1-24)	29.13 ± 4.72	1.00	*
H4K5acK8acK12ac (1-24)	78.30 ± 2.92	1.00	6.44 ± 1.78
H4K5acK12acK16ac (1-24)	34.06 ± 6.31	1.00	7.84 ± 1.04
H4K8acK12acK16ac (1-24)	47.83 ± 7.22	1.00	25.18 ± 2.69
H4K5acK8acK12acK16ac (1-24)	62.77 ± 10.93	0.99	27.24 ± 4.11
H4S1phK5ac (1-15)	84.21 ± 13.12	1.00	*
H4R3me2K5ac (1-24)	55.50 ± 11.20	1.08	*
H4K5acK8me1K12ac (1-24)	48.23 ± 2.44	0.927	*
H4K5acK8me1K12acK16ac (1-24)	47.93 ± 1.44	1.00	*
H4K16acK20me3 (1-24)	No Binding	NA	*

NA- Not applicable, *- Below detection limits

Table 2: Binding affinities of the ATAD2B bromodomain with the histone H4 oncohistone peptides that also carry an acetyllysine modification on K5 as measured by ITC. The apparent dissociation constants (K_D) are given in micromolar. Amino acid mutations are highlighted in the sequence.

Peptide Name	Peptide Sequence	Dissociation Constant, K_D (μM)	N
H4K5ac (1-15)[21]	SGRG(Kac)GGKGLGKGGA	5.2 ± 1.0	1.00
H4S1CK5ac (1-15)	**C**GRG(Kac)GGKGLGKGGA	19.40 ± 2.91	1.00
H4R3CK5ac (1-15)	SG**C**G(Kac)GGKGLGKGGA	22.90 ± 1.41	1.07
H4G4DK5ac (1-15)	SGR**D**(Kac)GGKGLGKGGA	No Binding	NA
H4G4SK5ac (1-15)	SGR**S**(Kac)GGKGLGKGGA	No Binding	NA

NA- Not applicable.

REFERENCES

1. Van Holde, K.E., Sahasrabuddhe, C.G. and Shaw, B.R. (1974) A model for particulate structure in chromatin. *Nucleic Acids Res*, **1**, 1579-1586.
2. Luger, K., Mader, A.W., Richmond, R.K., Sargent, D.F. and Richmond, T.J. (1997) Crystal structure of the nucleosome core particle at 2.8 A resolution. *Nature*, **389**, 251-260.
3. McGinty, R.K. and Tan, S. (2015) Nucleosome structure and function. *Chem Rev*, **115**, 2255-2273.
4. Sterner, D.E. and Berger, S.L. (2000) Acetylation of histones and transcription-related factors. *Microbiol Mol Biol Rev*, **64**, 435-459.
5. Millan-Zambrano, G., Burton, A., Bannister, A.J. and Schneider, R. (2022) Histone post-translational modifications - cause and consequence of genome function. *Nat Rev Genet*, **23**, 563-580.
6. Jenuwein, T. and Allis, C.D. (2001) Translating the histone code. *Science*, **293**, 1074-1080.
7. Franklin, K.A., Shields, C.E. and Haynes, K.A. (2022) Beyond the marks: reader-effectors as drivers of epigenetics and chromatin engineering. *Trends Biochem Sci*, **47**, 417-432.
8. Rothbart, S.B. and Strahl, B.D. (2014) Interpreting the language of histone and DNA modifications. *Biochim Biophys Acta*, **1839**, 627-643.
9. Zeng, L. and Zhou, M.M. (2002) Bromodomain: an acetyl-lysine binding domain. *FEBS Lett*, **513**, 124-128.
10. Grunstein, M. (1997) Histone acetylation in chromatin structure and transcription. *Nature*, **389**, 349-352.
11. Bannister, A.J. and Kouzarides, T. (2011) Regulation of chromatin by histone modifications. *Cell Research*, **21**, 381-395.
12. Nitsch, S., Zorro Shahidian, L. and Schneider, R. (2021) Histone acylations and chromatin dynamics: concepts, challenges, and links to metabolism. *EMBO Rep*, **22**, e52774.
13. Yang, X.J. and Seto, E. (2008) Lysine acetylation: codified crosstalk with other posttranslational modifications. *Mol Cell*, **31**, 449-461.
14. Bowman, G.D. and Poirier, M.G. (2015) Post-translational modifications of histones that influence nucleosome dynamics. *Chem Rev*, **115**, 2274-2295.
15. Mellor, J. (2006) It takes a PHD to read the histone code. *Cell*, **126**, 22-24.
16. Boyson, S.P., Gao, C., Quinn, K., Boyd, J., Paculova, H., Frietze, S. and Glass, K.C. (2021) Functional Roles of Bromodomain Proteins in Cancer. *Cancers (Basel)*, **13**.
17. Leachman, N.T., Brellier, F., Ferralli, J., Chiquet-Ehrismann, R. and Tucker, R.P. (2010) ATAD2B is a phylogenetically conserved nuclear protein expressed during neuronal differentiation and tumorigenesis. *Development, growth & differentiation*, **52**, 747-755.
18. Caron, C., Lestrat, C., Marsal, S., Escoffier, E., Curtet, S., Virolle, V., Barbry, P., Debernardi, A., Brambilla, C., Brambilla, E. *et al.* (2010) Functional characterization of ATAD2 as a new cancer/testis factor and a predictor of poor prognosis in breast and lung cancers. *Oncogene*, **29**, 5171-5181.

19. Koo, S.J., Fernandez-Montalvan, A.E., Badock, V., Ott, C.J., Holton, S.J., von Ahsen, O., Toedling, J., Vittori, S., Bradner, J.E. and Gorjanacz, M. (2016) ATAD2 is an epigenetic reader of newly synthesized histone marks during DNA replication. *Oncotarget*, **7**, 70323-70335.
20. Morozumi, Y., Boussouar, F., Tan, M., Chaikuad, A., Jamshidikia, M., Colak, G., He, H., Nie, L., Petosa, C., de Dieuleveult, M. *et al.* (2016) Atad2 is a generalist facilitator of chromatin dynamics in embryonic stem cells. *Journal of molecular cell biology*, **8**, 349-362.
21. Lloyd, J.T., McLaughlin, K., Lubula, M.Y., Gay, J.C., Dest, A., Gao, C., Phillips, M., Tonelli, M., Cornilescu, G., Marunde, M.R. *et al.* (2020) Structural Insights into the Recognition of Mono- and Diacetylated Histones by the ATAD2B Bromodomain. *J Med Chem*, **63**, 12799-12813.
22. Sobel, R.E., Cook, R.G., Perry, C.A., Annunziato, A.T. and Allis, C.D. (1995) Conservation of deposition-related acetylation sites in newly synthesized histones H3 and H4. *Proc Natl Acad Sci U S A*, **92**, 1237-1241.
23. Kabsch, W. (2010) Xds. *Acta Crystallogr D Biol Crystallogr*, **66**, 125-132.
24. McCoy, A.J., Grosse-Kunstleve, R.W., Adams, P.D., Winn, M.D., Storoni, L.C. and Read, R.J. (2007) Phaser crystallographic software. *Journal of applied crystallography*, **40**, 658-674.
25. Filippakopoulos, P., Picaud, S., Mangos, M., Keates, T., Lambert, J.P., Barsyte-Lovejoy, D., Felletar, I., Volkmer, R., Muller, S., Pawson, T. *et al.* (2012) Histone recognition and large-scale structural analysis of the human bromodomain family. *Cell*, **149**, 214-231.
26. Adams, P.D., Afonine, P.V., Bunkoczi, G., Chen, V.B., Davis, I.W., Echols, N., Headd, J.J., Hung, L.W., Kapral, G.J., Grosse-Kunstleve, R.W. *et al.* (2010) PHENIX: a comprehensive Python-based system for macromolecular structure solution. *Acta Crystallogr D Biol Crystallogr*, **66**, 213-221.
27. Emsley, P. and Cowtan, K. (2004) Coot: model-building tools for molecular graphics. *Acta Crystallogr D Biol Crystallogr*, **60**, 2126-2132.
28. Chen, V.B., Arendall, W.B., 3rd, Headd, J.J., Keedy, D.A., Immormino, R.M., Kapral, G.J., Murray, L.W., Richardson, J.S. and Richardson, D.C. (2010) MolProbity: all-atom structure validation for macromolecular crystallography. *Acta Crystallogr D Biol Crystallogr*, **66**, 12-21.
29. Adasme, M.F., Linnemann, K.L., Bolz, S.N., Kaiser, F., Salentin, S., Haupt, V.J. and Schroeder, M. (2021) PLIP 2021: expanding the scope of the protein-ligand interaction profiler to DNA and RNA. *Nucleic Acids Res*, **49**, W530-W534.
30. Holt, M.V., Wang, T. and Young, N.L. (2021) Expeditious Extraction of Histones from Limited Cells or Tissue Samples and Quantitative Top-Down Proteomic Analysis. *Curr Protoc*, **1**, e26.
31. DiMaggio, P.A., Jr., Young, N.L., Baliban, R.C., Garcia, B.A. and Floudas, C.A. (2009) A mixed integer linear optimization framework for the identification and quantification of targeted post-translational modifications of highly modified proteins using multiplexed electron transfer dissociation tandem mass spectrometry. *Mol Cell Proteomics*, **8**, 2527-2543.
32. Zhu, Q., Liu, N., Orkin, S.H. and Yuan, G.C. (2019) CUT&RUNTools: a flexible pipeline for CUT&RUN processing and footprint analysis. *Genome Biol*, **20**, 192.

33. Langmead, B. and Salzberg, S.L. (2012) Fast gapped-read alignment with Bowtie 2. *Nature methods*, **9**, 357-359.
34. Zhang, Y., Liu, T., Meyer, C.A., Eeckhoute, J., Johnson, D.S., Bernstein, B.E., Nusbaum, C., Myers, R.M., Brown, M., Li, W. *et al.* (2008) Model-based analysis of ChIP-Seq (MACS). *Genome biology*, **9**, R137.
35. Boyd, J., Rodriguez, P., Schjerven, H. and Frietze, S. (2021) ssvQC: an integrated CUT&RUN quality control workflow for histone modifications and transcription factors. *BMC Res Notes*, **14**, 366.
36. Ross-Innes, C.S., Stark, R., Teschendorff, A.E., Holmes, K.A., Ali, H.R., Dunning, M.J., Brown, G.D., Gojis, O., Ellis, I.O., Green, A.R. *et al.* (2012) Differential oestrogen receptor binding is associated with clinical outcome in breast cancer. *Nature*, **481**, 389-393.
37. Consortium, E.P. (2012) An integrated encyclopedia of DNA elements in the human genome. *Nature*, **489**, 57-74.
38. Luo, Y., Hitz, B.C., Gabdank, I., Hilton, J.A., Kagda, M.S., Lam, B., Myers, Z., Sud, P., Jou, J., Lin, K. *et al.* (2020) New developments on the Encyclopedia of DNA Elements (ENCODE) data portal. *Nucleic Acids Res*, **48**, D882-D889.
39. Aebersold, R., Agar, J.N., Amster, I.J., Baker, M.S., Bertozzi, C.R., Boja, E.S., Costello, C.E., Cravatt, B.F., Fenselau, C., Garcia, B.A. *et al.* (2018) How many human proteoforms are there? *Nat Chem Biol*, **14**, 206-214.
40. Jiang, T., Hoover, M.E., Holt, M.V., Freitas, M.A., Marshall, A.G. and Young, N.L. (2018) Middle-Down Characterization of the Cell Cycle Dependence of Histone H4 Posttranslational Modifications and Proteoforms. *Proteomics*, **18**, e1700442.
41. Leroy, G., Dimaggio, P.A., Chan, E.Y., Zee, B.M., Blanco, M.A., Bryant, B., Flaniken, I.Z., Liu, S., Kang, Y., Trojer, P. *et al.* (2013) A quantitative atlas of histone modification signatures from human cancer cells. *Epigenetics Chromatin*, **6**, 20.
42. Taylor, B.C. and Young, N.L. (2021) Combinations of histone post-translational modifications. *Biochem J*, **478**, 511-532.
43. Wang, T., Holt, M.V. and Young, N.L. (2018) The histone H4 proteoform dynamics in response to SUV4-20 inhibition reveals single molecule mechanisms of inhibitor resistance. *Epigenetics Chromatin*, **11**, 29.
44. Evans, C.M., Phillips, M., Malone, K.L., Tonelli, M., Cornilescu, G., Cornilescu, C., Holton, S.J., Gorjanacz, M., Wang, L., Carlson, S. *et al.* (2021) Coordination of Di-Acetylated Histone Ligands by the ATAD2 Bromodomain. *Int J Mol Sci*, **22**.
45. Nacev, B.A., Feng, L., Bagert, J.D., Lemiesz, A.E., Gao, J., Soshnev, A.A., Kundra, R., Schultz, N., Muir, T.W. and Allis, C.D. (2019) The expanding landscape of 'oncohistone' mutations in human cancers. *Nature*, **567**, 473-478.
46. Amatori, S., Tavolaro, S., Gambardella, S. and Fanelli, M. (2021) The dark side of histones: genomic organization and role of oncohistones in cancer. *Clin Epigenetics*, **13**, 71.
47. Mjelle, R., Hegre, S.A., Aas, P.A., Slupphaug, G., Drablos, F., Saetrom, P. and Krokan, H.E. (2015) Cell cycle regulation of human DNA repair and chromatin remodeling genes. *DNA Repair (Amst)*, **30**, 53-67.

48. Liu, Q., Liu, H., Huang, X., Fan, X., Xiao, Z., Yan, R., Yao, J., An, G., Ge, Y., Miao, J. *et al.* (2022) A targetable MYBL2-ATAD2 axis governs cell proliferation in ovarian cancer. *Cancer Gene Ther*.
49. Lazarchuk, P., Hernandez-Villanueva, J., Pavlova, M.N., Federation, A., MacCoss, M. and Sidorova, J.M. (2020) Mutual Balance of Histone Deacetylases 1 and 2 and the Acetyl Reader ATAD2 Regulates the Level of Acetylation of Histone H4 on Nascent Chromatin of Human Cells. *Mol Cell Biol*, **40**.
50. Jiang, Y., Hu, T., Wang, T., Shi, X., Kitano, A., Eagle, K., Hoegenauer, K.A., Konopleva, M.Y., Lin, C.Y., Young, N.L. *et al.* (2019) AMP-activated protein kinase links acetyl-CoA homeostasis to BRD4 recruitment in acute myeloid leukemia. *Blood*, **134**, 2183-2194.
51. Hammond, C.M., Stromme, C.B., Huang, H., Patel, D.J. and Groth, A. (2017) Histone chaperone networks shaping chromatin function. *Nature reviews. Molecular cell biology*, **18**, 141-158.
52. Alabert, C., Bukowski-Wills, J.C., Lee, S.B., Kustatscher, G., Nakamura, K., de Lima Alves, F., Menard, P., Mejlvang, J., Rappsilber, J. and Groth, A. (2014) Nascent chromatin capture proteomics determines chromatin dynamics during DNA replication and identifies unknown fork components. *Nat Cell Biol*, **16**, 281-293.
53. Garcia, B.A., Shabanowitz, J. and Hunt, D.F. (2007) Characterization of histones and their post-translational modifications by mass spectrometry. *Curr Opin Chem Biol*, **11**, 66-73.
54. Bonisch, C., Nieratschker, S.M., Orfanos, N.K. and Hake, S.B. (2008) Chromatin proteomics and epigenetic regulatory circuits. *Expert Rev Proteomics*, **5**, 105-119.
55. Barlesi, F., Giaccone, G., Gallegos-Ruiz, M.I., Loundou, A., Span, S.W., Lefesvre, P., Kruyt, F.A. and Rodriguez, J.A. (2007) Global histone modifications predict prognosis of resected non small-cell lung cancer. *J Clin Oncol*, **25**, 4358-4364.
56. Burlingame, A.L., Zhang, X. and Chalkley, R.J. (2005) Mass spectrometric analysis of histone posttranslational modifications. *Methods*, **36**, 383-394.
57. Su, X., Ren, C. and Freitas, M.A. (2007) Mass spectrometry-based strategies for characterization of histones and their post-translational modifications. *Expert Rev Proteomics*, **4**, 211-225.
58. Ruiz-Carrillo, A., Wangh, L.J. and Allfrey, V.G. (1975) Processing of newly synthesized histone molecules. *Science*, **190**, 117-128.
59. Barber, C.M., Turner, F.B., Wang, Y., Hagstrom, K., Taverna, S.D., Mollah, S., Ueberheide, B., Meyer, B.J., Hunt, D.F., Cheung, P. *et al.* (2004) The enhancement of histone H4 and H2A serine 1 phosphorylation during mitosis and S-phase is evolutionarily conserved. *Chromosoma*, **112**, 360-371.
60. Cheung, W.L., Turner, F.B., Krishnamoorthy, T., Wolner, B., Ahn, S.H., Foley, M., Dorsey, J.A., Peterson, C.L., Berger, S.L. and Allis, C.D. (2005) Phosphorylation of histone H4 serine 1 during DNA damage requires casein kinase II in S. cerevisiae. *Curr Biol*, **15**, 656-660.
61. Fischle, W., Tseng, B.S., Dormann, H.L., Ueberheide, B.M., Garcia, B.A., Shabanowitz, J., Hunt, D.F., Funabiki, H. and Allis, C.D. (2005) Regulation of HP1-chromatin binding by histone H3 methylation and phosphorylation. *Nature*, **438**, 1116-1122.

62. Poncet-Montange, G., Zhan, Y., Bardenhagen, J.P., Petrocchi, A., Leo, E., Shi, X., Lee, G.R.t., Leonard, P.G., Geck Do, M.K., Cardozo, M.G. *et al.* (2015) Observed bromodomain flexibility reveals histone peptide- and small molecule ligand-compatible forms of ATAD2. *Biochem J*, **466**, 337-346.
63. Wolffe, A.P. and Hayes, J.J. (1999) Chromatin disruption and modification. *Nucleic Acids Res*, **27**, 711-720.
64. Tse, C., Sera, T., Wolffe, A.P. and Hansen, J.C. (1998) Disruption of higher-order folding by core histone acetylation dramatically enhances transcription of nucleosomal arrays by RNA polymerase III. *Mol Cell Biol*, **18**, 4629-4638.
65. Allahverdi, A., Yang, R., Korolev, N., Fan, Y., Davey, C.A., Liu, C.F. and Nordenskiold, L. (2011) The effects of histone H4 tail acetylations on cation-induced chromatin folding and self-association. *Nucleic Acids Res*, **39**, 1680-1691.
66. Dhar, S., Gursoy-Yuzugullu, O., Parasuram, R. and Price, B.D. (2017) The tale of a tail: histone H4 acetylation and the repair of DNA breaks. *Philos Trans R Soc Lond B Biol Sci*, **372**.

FIGURES

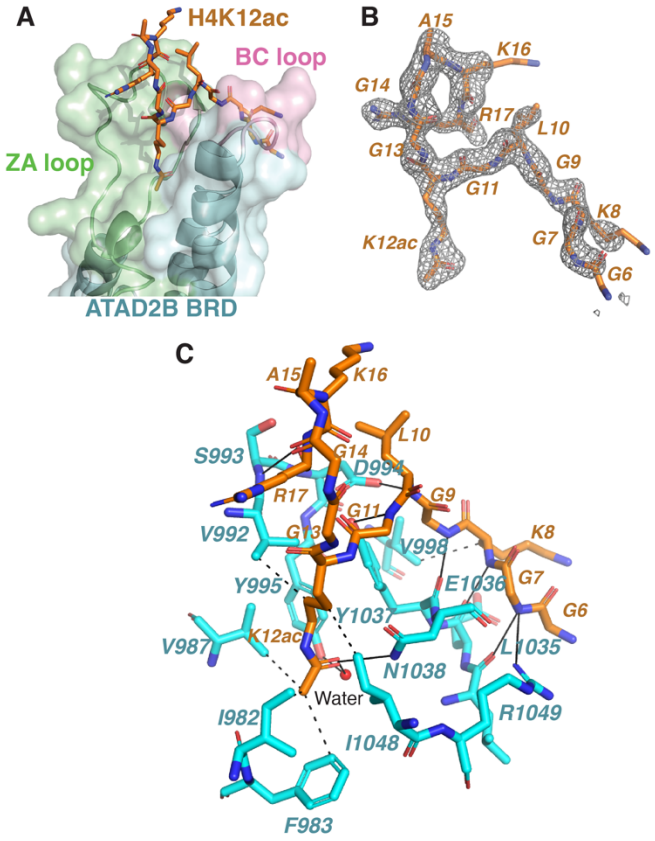

Figure 1: Coordination of the histone H4K12ac ligand by the ATAD2B bromodomain. (A) A surface representation of the ATAD2B BRD in complex with the H4K12ac ligand (residues 4-17) (PDB ID: 8EOQ). The H4K12ac ligand residues are shown as orange sticks, while the cartoon representation of BRD (cyan) highlights the ZA and BC loops in green and pink, respectively. (B) An isolated image of the simulated annealing composite omit map (gray) around the histone ligand H4K12ac (orange) contoured at 1σ. The composite omit map was calculated before building the histone ligand into the structure. All figures were made using the PyMOL Molecular Graphics system using version 2.3, Schrödinger, LLC. (C) Coordination of the H4K12ac ligand by the ATAD2B BRD. Residues lining the BRD pocket that are involved in ligand coordination are displayed in cyan, while the H4K12ac ligand residues are in orange. Hydrogen bond contacts are represented by a solid black line, and hydrophobic interactions are shown by dashed black lines. All contacts were determined using the PLIP program (29).

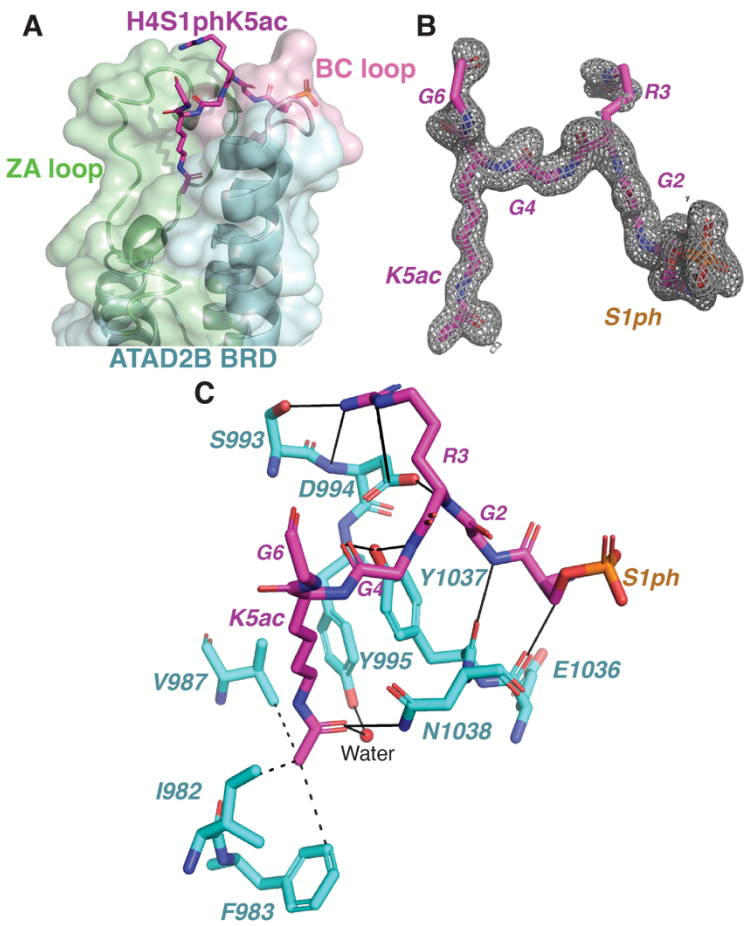

Figure 2: Coordination of the histone H4S1phK5ac ligand by the ATAD2B bromodomain. (A) A surface representation of the ATAD2B BRD in complex with the H4S1phK5ac ligand (residues 1-15) (PDB ID: 8ESJ). The H4S1phK5ac ligand residues are shown as pink sticks, while cartoon representation of BRD (cyan) highlights the ZA and BC loops are in green and pink, respectively. (B) An isolated image of the simulated annealing composite omit map (gray) around the histone ligand H4S1phK5ac (magenta) contoured at 1σ. The composite omit map was calculated before building the histone ligand into the structure. All figures were made using the PyMOL Molecular Graphics system using version 2.3, Schrödinger, LLC. (C) Coordination of the H4S1phK5ac ligand by the ATAD2 BRD. Residues lining the BRD pocket that are involved in ligand coordination are displayed in cyan, while the H4S1phK5ac ligand residues are in magenta. Hydrogen bond contacts are represented by a solid black line and hydrophobic interactions are shown by dashed black lines. All contacts were determined using the PLIP program (29).

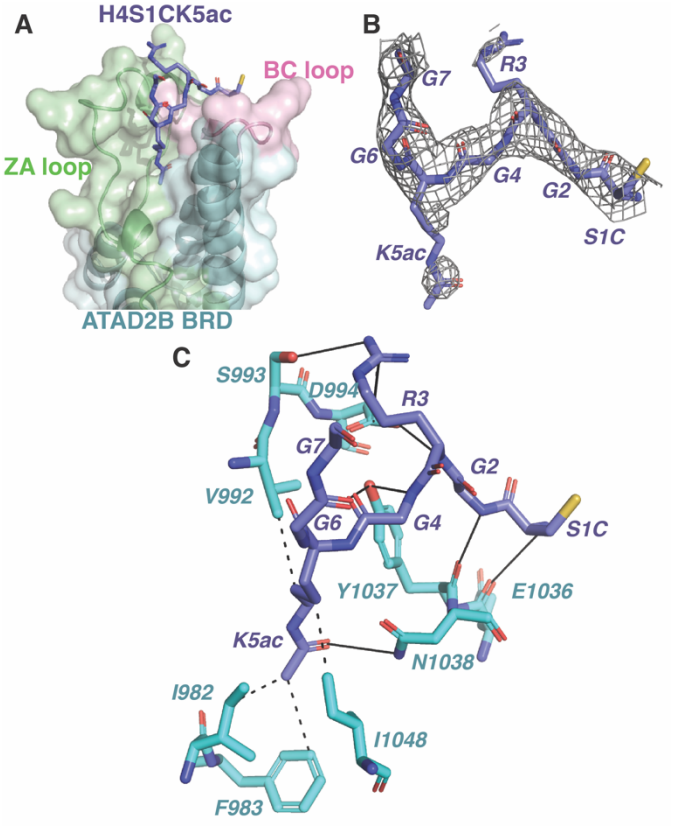

Figure 3: Coordination of the oncohistone H4S1CK5ac ligand by the ATAD2B bromodomain. (A) A surface representation of the ATAD2B BRD in complex with the H4S1CK5ac ligand (residues 1-15) (PDB ID: 7ZTQ). The H4S1CK5ac ligand residues are shown as purple sticks, while the cartoon representation of BRD (cyan) highlights the ZA and BC loops in green and pink, respectively. (B) An isolated image of the simulated annealing composite omit map (gray) around the histone ligand H4S1CK5ac (purple) contoured at 1σ. The composite omit map was calculated before building the histone ligand into the structure. All figures were made using the PyMOL Molecular Graphics system using version 2.3, Schrödinger, LLC. (C) Coordination of the H4S1CK5ac ligand by the ATAD2 BRD. Residues lining the BRD pocket that are involved in ligand coordination are displayed in cyan, while the H4S1CK5ac ligand residues are in purple. Hydrogen bond contacts are represented by a solid black line and hydrophobic interactions are shown by dashed black lines. All contacts were determined using the PLIP program (29).

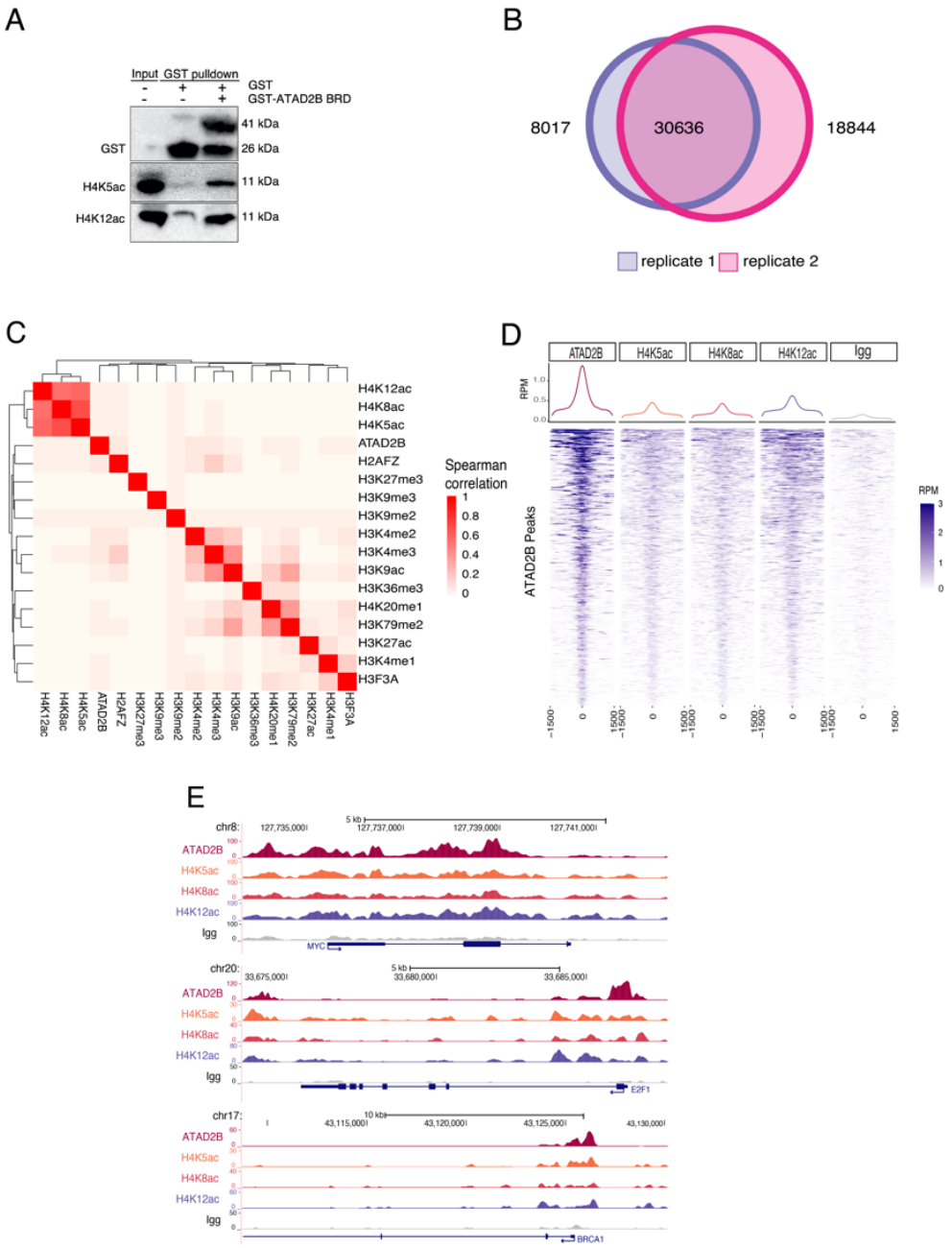

Figure 4: ATAD2B is enriched with genomic sites of acetylated lysine on histone H4. (A) Immunoblot showing the interaction of GST-tagged ATAD2B BRD (41 kDa) with endogenous histone H4 (15 kDa) from MCF7 cells. Recombinant GST alone was used as a control. Specific antibodies were used for the GST tag, and the H4K5ac and H4K12ac modifications. (B) Euler plot showing strong replicate concordance for ATAD2B CUT&RUN samples. A total of 30,636 high-confidence peaks were identified across two biological replicates for ATAD2B. (C) Correlation heatmap based on comparing ATAD2B and our H4Kac PTM CUT&RUN data against all public ChIP-seq data for histone modifications in the breast cancer cell line MCF7. Clustering is derived from the Euclidian distance of signalValue for each factor and shows a strong correlation between ATAD2B and the H4Kac PTMs. (D) Signal heat map of CUT&RUN signals for all factors at the ATAD2B high-confidence peaks, showing strong signal correlation for histone H4Kac PTMs with the signal at ATAD2B peaks. (E) UCSC genome browser snapshots of CUT&RUN signal (reads per kilo-million) on multiple breast cancer-related genes (MYC, E2F1, BRCA1).

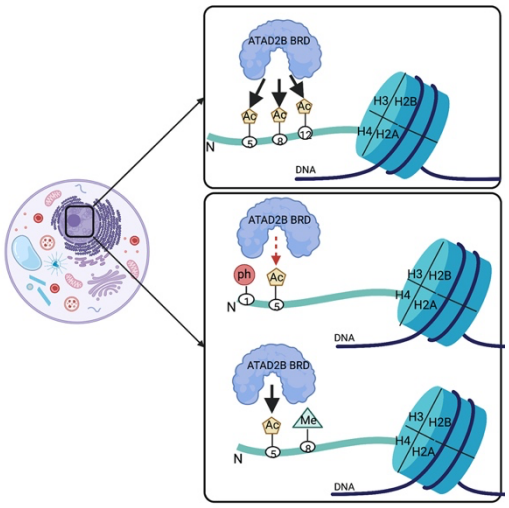

Figure 5: Proposed mechanism for the histone code modulation of the ATAD2B bromodomain activity. In the cell, ATAD2B is localized at the chromatin which is enriched with acetylation marks. The top panel shows the BRD engaging with the acetylation marks. The presence of adjacent post-translational modifications also influences the BRD activity of ATAD2B. The phosphoryl group at the N-terminus of the histone H4 tail negatively impacts recognition of the adjacent acetyllysine group by the ATAD2B BRD (middle), whereas methyl groups have little effect on the adjacent acetyllysine recognition (bottom). Thus, recognition of acetyllysine by the ATAD2B BRD is mediated by the presence of multiple modifications on individual histone tails of the nucleosome.